Chinese Journal of Natural Medicines

Ramulus Mori alkaloids (SZ-A) sensitize triple-negative breast cancer to cisplatin *via* PLA2G2A-mediated ceramide metabolism

Chao Chen, Mengqi Wan, Zhixu Zhu, Zhaoyu Xie, Yu Zhang, Tao Xu, Han Meng, Miaomiao Wu, Liangfeng Gui, Hongbo Lv, Guodong Wang, Jun Han, Hui Che

Citation: Chao Chen, Mengqi Wan, Zhixu Zhu, Zhaoyu Xie, Yu Zhang, Tao Xu, Han Meng, Miaomiao Wu, Liangfeng Gui, Hongbo Lv, Guodong Wang, Jun Han, Hui Che, Ramulus Mori alkaloids (SZ-A) sensitize triple-negative breast cancer to cisplatin *via* PLA2G2A-mediated ceramide metabolism, Chinese Journal of Natural Medicines, 2026, 24(8), 972-986. doi: 10.1016/S1875-5364(26)61196-X.

View online: https://doi.org/10.1016/S1875-5364(26)61196-X

Related articles that may interest you

Design, synthesis, and biological evaluation of novel chrysin derivatives as poly(ADP-ribose) polymerase 1 (PARP1) inhibitors for the treatment of breast cancer

Chinese Journal of Natural Medicines. 2024, 22(5), 455-465 https://doi.org/10.1016/S1875-5364(24)60642-4

Panax notoginseng saponins prevent colitis-associated colorectal cancer *via* inhibition IDO1 mediated immune regulation

Chinese Journal of Natural Medicines. 2022, 20(4), 258-269 https://doi.org/10.1016/S1875-5364(22)60179-1

Polyphyllin I promotes cell death *via* suppressing UPR-mediated CHOP ubiquitination and degradation in non-small cell lung cancer

Chinese Journal of Natural Medicines. 2021, 19(4), 255-266 https://doi.org/10.1016/S1875-5364(21)60027-4

A systematic review of pharmacological activities, toxicological mechanisms and pharmacokinetic studies on *Aconitum* alkaloids

Chinese Journal of Natural Medicines. 2021, 19(7), 505-520 https://doi.org/10.1016/S1875-5364(21)60050-X

Bavachin induces apoptosis in colorectal cancer cells through Gadd45a *via* the MAPK signaling pathway

Chinese Journal of Natural Medicines. 2023, 21(1), 36-46 https://doi.org/10.1016/S1875-5364(23)60383-8

Therapeutic potential of alkaloid extract from Codonopsis Radix in alleviating hepatic lipid accumulation: insights into mitochondrial energy metabolism and endoplasmic reticulum stress regulation in NAFLD mice

Chinese Journal of Natural Medicines. 2023, 21(6), 411-422 https://doi.org/10.1016/S1875-5364(23)60403-0

Wechat

Chinese Journal of Natural Medicines 24 (2026) 972-986

Contents lists available at ScienceDirect

Chinese Journal of Natural Medicines

journal homepage: www.cjnmcpu.com/

Original article

Ramulus Mori alkaloids (SZ-A) sensitize triple-negative breast cancer to cisplatin *via* PLA2G2A-mediated ceramide metabolism

Chao Chen[a,b,Δ], Mengqi Wan[a,b,Δ], Zhixu Zhu[a,b], Zhaoyu Xie[a,b], Yu Zhang[a,b], Tao Xu[a,b], Han Meng[a,b], Miaomiao Wu[a,b], Liangfeng Gui[a,b], Hongbo Lv[a,b], Guodong Wang[a,b,*], Jun Han[c,*], Hui Che[a,c,d,*]

[a] *Department of Pharmacology, Wannan Medical College, Wuhu 241002, China*
[b] *Anhui Innovative Center for Drug Basic Research of Metabolic Diseases, Wannan Medical College, Wuhu 241002, China*
[c] *Wuhu Modern Technology Research and Development Center of Chinese Herbal Medicine and Functional Food, Anhui College of Traditional Chinese Medicine, Wuhu 241002, China*
[d] *Department of Endocrinology and Genetic Metabolism, The First Affiliated Hospital of Wannan Medical College (Yijishan Hospital of Wannan Medical College), Wuhu 241002, China*

ARTICLE INFO

Article history:
Received 10 November 2025
Revised 22 December 2025
Accepted 19 January 2026
Available online 20 August 2026

Keywords:
Ramulus Mori alkaloids
Triple-negative breast cancer (TNBC)
Cisplatin
Phospholipase A2 Group IIA (PLA2G2A)
Ceramide

ABSTRACT

Cisplatin (DDP) remains a standard therapy for triple-negative breast cancer (TNBC), yet intrinsic or acquired resistance often limits its efficacy; here, we report that Ramulus Mori alkaloids (SZ-A), an approved botanical *α*-glucosidase inhibitors, synergize with DDP to suppress TNBC progression *in vitro* and *in vivo* by driving PLA2G2A-dependent ceramide accumulation. Combining SZ-A with DDP synergistically inhibits viability, clonogenicity, migration, and invasion, induces S-phase arrest and apoptosis, and attenuates tumor growth in xenograft models. Mechanistically, SZ-A directly binds to and stabilizes PLA2G2A, blocking its autophagic-lysosomal degradation, leading to accumulated PLA2G2A that suppresses fatty acid oxidation and triggers ceramide accrual *via* ADIPOR2 inhibition. Genetic ablation of PLA2G2A abrogates these effects. DDP further enhances SZ-A-induced PLA2G2A upregulation and ceramide accumulation, resulting amplified cytotoxicity. Our findings reveal SZ-A as a chemosensitizing agent that enhances the efficacy of DDP in TNBC.

1. Introduction

Triple-negative breast cancer (TNBC) represents a particularly aggressive subtype of breast cancer, characterized by the absence of estrogen receptor (ER), progesterone receptor (PR), and human epidermal growth factor receptor 2 (HER2) expression [1]. Owing to its inherent resistance to conventional endocrine and targeted therapies, TNBC treatment predominantly depends on chemotherapy, with cisplatin (DDP) being among the most frequently employed agents [2]. Nonetheless, the therapeutic effectiveness of DDP is frequently constrained by the emergence of drug resistance and notable adverse effects. Consequently, investigating innovative adjuvant strategies to augment the efficacy of DDP while mitigating its toxicity is of paramount importance for enhancing the prognosis of patients with TNBC.

Natural products serve as a prolific source of anti-tumor agents, employing multi-target mechanisms to interfere with carcinogenic pathways [3]. Bioactive compounds derived from traditional medicinal plants, such as Ramulus Mori (Sangzhi, SZ), have demonstrated significant potential. It is indicated that polysaccharides extracted from SZ can induce apoptosis in ovarian and gastric cancer cells [4]. Furthermore, a distinct alkaloid component found in SZ, known as Ramulus Mori alkaloid (SZ-A), which includes piperidine alkaloid 1-deoxynojirimycin (DNJ), 1,4-dideoxy-1,4-imino-D-arabinitol (DAB) and fargomine (FA), has received clinical approval for the treatment of type 2 diabetes mellitus (T2DM) [5]. SZ-A primarily exerts its hypoglycemic effects through potent inhibition of *α*-glucosidase and modulation of lipid metabolism. Emerging evidence also suggests that SZ-A ameliorates metabolic disorders, including obesity and atherosclerosis, *via* mechanisms involving the remodeling of intestinal microbiota, bile acid signaling, and the inhibition of inflammatory cascades [6-8].

Lipid metabolism reprogramming is a critical hallmark of cancer progression and serves as a key mediator of chemotherapy resistance in TNBC [9]. Considering the established role of SZ-A in regulating systemic lipid homeostasis and its pleiotropic effects on interconnected metabolic and inflammatory networks, we propose that SZ-A may target tumor-specific metabolic vulnerabilities to enhance the efficacy of chemotherapy. Nevertheless, the capacity of SZ-A to modulate lipid metabolism within the TNBC microenvironment, thereby sensitizing tumors to cytotoxic agents, and the potential molecular determinants of this interaction remain entirely unexplored.

Secreted phospholipase A2 group IIA (PLA2G2A), a catalytically active hydrolase that liberates fatty acids and bioactive lipids from membrane phospholipids, orchestrates fundamental processes including membrane remodeling, cell death execution,

* Corresponding author.
E-mail addresses: wangguodong@wnmc.edu.cn (G. Wang); hanjun@wnmc.edu.cn (J. Han); chehui1203@163.com (H. Che)
Δ These authors contributed equally to this work.

https://doi.org/10.1016/S1875-5364(26)61196-X
Copyright © 2026, China Pharmaceutical University. Published by Elsevier B.V. All rights are reserved.

lipid mediator production, and inflammatory cytokine secretion [10, 11]. Despite its well-defined biochemical functions, PLA2G2A exhibits a paradoxical role in oncogenesis. In lung and prostate cancer, elevated PLA2G2A expression correlates with aggressive phenotypes and diminished patient survival [12-14]. Conversely, in gastric cancer, elevated PLA2G2A expression is linked to improved patient survival rates. The expression of PLA2G2A is inversely correlated with infiltration depth, lymph node metastasis, and the tumor-lymph node-metastasis stage [15, 16]. In breast cancer, where the plant alkaloid stachydrine triggers cell apoptosis through PLA2G2A upregulation [17], yet whether SZ-A modulates PLA2G2A to enhance DDP sensitivity in TNBC remains unexplored.

Herein, we establish that the combination of SZ-A and DDP exerts potent anti-tumor activity against TNBC. Mechanistically, SZ-A directly targets PLA2G2A, stabilizing it by inhibiting lysosomal degradation. This stabilization reprograms sphingolipid metabolism, driving ceramide accumulation and ultimately triggering TNBC cell apoptosis. The SZ-A/DDP combination synergistically amplifies the PLA2G2A-ceramide axis, thus defining a potent pharmacological strategy to chemosensitize refractory TNBC.

2. Materials and methods

2.1. Chemicals and antibodies

Anti-PLA2G2A (Cat. DF6366), Bcl-2 (Cat. AF6139), Bax (Cat. AF0120) and GAPDH (Cat. AF7021) antibodies were from Affinity Biosciences (Wuhan, China); anti-cleaved caspase-3 (Cat. 87055-4-RR) and Ki-67 (Cat. 27309-1-AP) from Proteintech (Wuhan, China). ADIPOR1/2 siRNAs, PLA2G2A overexpression plasmid, and shPLA2G2A lentivirus were obtained from GeneAdv Biotechnology (Suzhou, China). Pronase E (Cat. S10014) was sourced from Yuanye Bio-Technology (Shanghai, China); recombinant human TNF-α (Cat. DC008) from Novoprotein (Suzhou, China). Carmofur (Cat. C425087), chloroquine (Cat. C193834), MG132 (Cat. M408577) and cycloheximide (Cat. C408230) were purchased from Aladdin (Shanghai, China). Oil Red O (Cat. G1262) was from Solarbio (Beijing, China); BODIPY 493/503 was from Beyotime (Cat. C2053S, Nanjing, China).

2.2. Cell lines

MDA-MB-231 and BT-549 cells were obtained from the Cell Bank of the Shanghai Institute of Biochemistry and Cell Biology. BT-549 cells were maintained in RPMI-1640 (Cat. C11875500BT, Gibco, Suzhou, China) and MDA-MB-231 cells in DMEM (Cat. BL304A, Biosharp, Beijing, China), each supplemented with 10% fetal bovine serum (Cat. PWL217, MeilunBio, Dalian, China) and 1% penicillin–streptomycin (Cat. S0198, HaiGene, Harbin, China). Cultures were incubated at 37 °C in 5% CO_2/95% air with ≥ 95% humidity.

2.3. SZ-A preparation

SZ-A was provided by Wehand Biotech (Cat. J202207014, Beijing, China). The extract is characterized by its principal alkaloid constituents: DNJ, DAB and FA. HPLC analysis indicated a DNJ content of 39.3% and a total alkaloid content > 60%. Aliquots were stored at −80 °C until use.

2.4. Subcutaneous xenografts

MDA-MB-231 cells (2×10^6 cells/mouse) were subcutaneously inoculated into the right back of 4-week-old female BALB/c nude mice (Cavens, Changzhou, China, n = 8/group). When tumor volumes reached 100 mm^3 (calculated as length × $width^2/2$), mice were randomized into four treatment groups: Model, SZ-A (50 $mg \cdot kg^{-1}$, p.o.), DDP (2 $mg \cdot kg^{-1}$, i.p. every other day), and SZ-A/DDP combination. Tumor growth was monitored for 28 days. Terminal tumors were excised, weighed, and processed for further analysis. All procedures were approved by the Wannan Medical College Animal Ethics Committee (Approval No. WNMC-AWE-2025333) in compliance with ARRIVE guidelines.

2.5. Network pharmacology analysis

Putative targets of SZ-A bioactives (DNJ, FA, DAB) were retrieved from the SWISS Target Prediction platform (probability > 0.3). TNBC-relevant genes were mined from GeneCards, DisGeNET and OMIM; redundant entries were collapsed to a non-redundant disease gene set. Intersection of compound targets and disease genes defined the pharmacological focus set. Protein–protein interactions were imported into Cytoscape v3.9.1 to generate a compound–target–disease network, whose topological parameters were computed with NetworkAnalyzer. GO biological process and KEGG pathways annotation were performed with clusterProfiler v4.0.5 in R v4.1.1.

2.6. Molecular docking

Three-dimensional structures of DNJ, FA and DAB were downloaded from PubChem and the PLA2G2A crystal structure (ID: 3U8B) was retrieved from the RCSB Protein Data Bank. All ligands were energy-minimized with MMFF94, while the protein was protonated and stripped of crystallographic water and non-interacting ions. Blind molecular docking was performed by CB-Dock2 (https://cadd.labshare.cn/cb-dock2/php/index.php), and the results were visualized with PyMOL 2.6.

2.7. Quantitative RT-PCR

Total RNA was extracted with TRIzol reagent (Cat. 16096020, Invitrogen, Shanghai, China) and reverse-transcribed using the ReverTra Ace® qPCR-RT kit (Toyobo, Osaka, Japan) following the manufacturer's protocol. Quantitative PCR was performed on a CFX96 system (Bio-Rad, Shanghai, China) with SGExcel FastSYBR qPCR Mixture (Sangon Biotech, Shanghai, China) and gene-specific primers (Table S1). Relative expression was calculated by the $2^{(-\Delta\Delta Ct)}$ method, with β-actin as the endogenous reference gene.

2.8. Immunofluorescence

Cells or cryosections were washed in PBS, fixed with 4% paraformaldehyde, and permeabilized with 0.5% Triton X-100 for 10 min. After blocking with 5% goat serum, specimens were incubated overnight at 4 °C with anti-PLA2G2A and Ki67 primary antibodies. Following PBS washes, slides were probed with species-matched secondary antibodies (1∶1000, Beyotime, Shanghai, China) at 37 °C for 1 h and nuclei were counterstained with DAPI. Images were captured on a microscope (Eclipse Ni, Nikon, Tokyo, Japan).

2.9. Oil Red O staining

Cells were rinsed with PBS, fixed in 4% paraformaldehyde, washed with distilled water, and equilibrated with 60% isopropanol for 5 min. Lipid droplets were stained with freshly filtered Oil Red O working solution for 15 min, followed by three washes in distilled water to remove unbound dye. Images were acquired on a microscope .

2.10. Calcein/EthD cytotoxicity detection

Cell viability was evaluated with a calcein-AM/ethidium homodimer-III (EthD-III) dual-fluorophore (Solarbio, CA1632) assay. Chemically treated cells were incubated with calcein-AM (2 μmol·L^{-1}) and then exposed to EthD-III (4 μmol·L^{-1}) for 3 min at 37 °C. Live (green fluorescence, Ex/Em 490/515 nm) and dead (red fluorescence, Ex/Em 530/645 nm) cells were imaged on a microscope.

2.11. Transwell invasion assay

1 × 10^4 MDA-MB-231 or BT-549 cells were seeded in 8-μm transwell inserts pre-coated with matrigel, and treated with SZ-A, DDP, or their combination in serum-free medium. The lower chamber contained 500 μL complete medium. After 24–48 h at 37 °C, cells on the underside were fixed in 4% paraformaldehyde, stained with 0.1% crystal violet, and enumerated per insert under a light microscope.

2.12. Western blot

Proteins were extracted with RIPA buffer, quantified by BCA assay, and denatured in loading buffer. Equal amounts were resolved on SDS-PAGE gels and transferred to nitrocellulose membranes (Cat. FFN08, Beyotime, Shanghai, China). Membranes were blocked with 5% skim milk, incubated with primary antibodies, and probed with HRP-conjugated secondary antibodies (1∶8000, Cat. BA1054, Boster, WuHan, China). Immunoreactive bands were visualized using Image Quant 800 (Cytiva, MA, USA).

2.13. Wound-healing assay

MDA-MB-231 or BT-549 cells were plated in 6-well plates to ≥ 90% confluence. A uniform scratch was generated with a sterile tip, debris was removed by PBS wash, and cells were exposed to SZ-A, DDP, or the indicated combinations in serum-free medium. Images were acquired at 0, 12 and 24 h with an inverted microscope.

2.14. Flow cytometry

For analyzing the cell apoptosis, cells were trypsinized after treatment with SZ-A, DDP or the indicated agents, resuspended in 100 μL binding buffer and stained with Annexin V-FITC/PI (Annexin V-FITC/PI kit, Cat. XP018Pro-100, 4A Biotech, Suzhou, China) in the dark. Samples were diluted to 300 μL and analyzed on flow cytometer; Annexin V$^+$/PI$^-$ and Annexin V$^+$/PI$^+$ populations were recorded as early and late apoptotic cells.

For analyzing the cell cycle, cells were fixed in 70% ice-cold ethanol, washed and incubated with PI plus RNase A for 30 min in the dark. DNA content was acquired on a flow cytometer (BD FACSVerse, NJ, USA) and modeled using FlowJo.

2.15. TUNEL apoptosis detection

Paraffin-embedded xenograft sections were deparaffinized, rehydrated through graded ethanol, and subjected to antigen retrieval by microwaving in 10 mmol·L^{-1} sodium citrate (pH 6.0). Endogenous peroxidase activity was quenched with 3% H_2O_2. Sections were permeabilized with proteinase K, then labelled with the TUNEL reaction mixture (Cat. 40306ES20, Yeasen, Shanghai, China) at 37 °C for 60 min, and incubated with DAPI. The percentage of TUNEL-positive cells was quantified by ImageJ software.

2.16. Lipid metabolism quantification and lipidomics

Cell or tissue lysates prepared after the indicated treatments were subjected to colorimetric (FAO, Cat. E-BC-K784-M, Elabscience, Wuhan, China), fluorometric (FFAs, Cat. S0215S, Beyotime, Shanghai, China) and ELISA-based (ceramides, Cat. CB11256, Coibio, Shanghai, China) assays according to the manufacturers' protocols. Absorbance/fluorescence was read on a BioTek microplate reader against freshly generated standard curves to obtain absolute concentrations. Untargeted lipidomics was performed by Majorbio Biotech (Shanghai, China).

2.17. Cellular thermal shift assay (CETSA)

Cells were treated with SZ-A or vehicle control for 1 h prior to harvesting. Washed cells were resuspended RIPA buffers and aliquoted into PCR tubes. Samples were subjected to a temperature gradient (37, 43, 47, 55, 61 and 67 °C) for 3 min in a thermal cycler (Applied biosystems VeritiPro, Thermofisher, Shanghai, China). Lysates were clarified by centrifugation and PLA2G2A proteins in supernatants were detected by immunoblotting.

2.18. Statistical analysis

Statistical analyses were performed in GraphPad Prism 10.0.2. Data are expressed as mean ± SEM. Comparisons between two groups were assessed by two-tailed Student's *t*-test; multiple groups were evaluated using one-way ANOVA. $P < 0.05$ was considered statistically significant.

3. Result

3.1. SZ-A synergistically enhances DDP-induced apoptosis and suppresses malignant phenotypes in TNBC cells

To evaluate the cytotoxic effects of SZ-A on TNBC, BT-549 and MDA-MB-231 cells were exposed to graded concentrations of 10, 30, and 100 μg·mL^{-1}. Even at the 100 μg·mL^{-1} concentration, SZ-A did not reduce cell viability by more than 50% in either cell line, indicating limited monotherapeutic potential (Fig. 1A). These findings prompted exploration of SZ-A combination regimens with conventional chemotherapeutics to enhance antitumor activity. Consequently, combinatorial regimens with conventional chemotherapeutics were assessed. Co-treatment with SZ-A (50 μg·mL^{-1}) and DDP (2 μmol·L^{-1}) significantly decreased cell viability relative to either agent alone (Fig. 1B). The HSA synergy score for the SZ-A and DDP combination, calculated using SynergyFinder+, was 14.023, confirming a notable synergistic interaction (Fig. 1C). This combination dose induced > 50% cytotoxicity and was selected for subsequent mechanistic studies. SZ-A/DDP co-treatment induced S-phase cell cycle arrest in both TNBC lines, significantly suppressing proliferation (Figs. 1D and 1E). Consistently, EdU incorporation and Ki-67 expression were markedly reduced (Figs. 1F–1I), and clonogenic survival was diminished by > 70% (Figs. 1J and 1K), collectively indicating impaired proliferative capacity.

Furthermore, the combination significantly increased dead (Ethd-III$^+$) and apoptotic (Annexin V$^+$/PI$^+$) cell populations and modulated key apoptotic markers: upregulation of Bax and cleaved caspase-3, with concomitant Bcl-2 downregulation (Figs. 2A–2E). Functional assays demonstrated that SZ-A/DDP co-treatment also significantly inhibited migration and invasion in both cell lines (Figs. 2F–2I). These data demonstrate that SZ-A potentiates DDP-mediated cytotoxicity in TNBC cells *in vitro*.

3.2. PLA2G2A is identified as a central mediator of SZ-A-induced apoptosis in TNBC

To identify molecular targets of SZ-A in TNBC, we integrated network pharmacology with pathway enrichment analysis. Target genes associated with TNBC were systematically retrieved

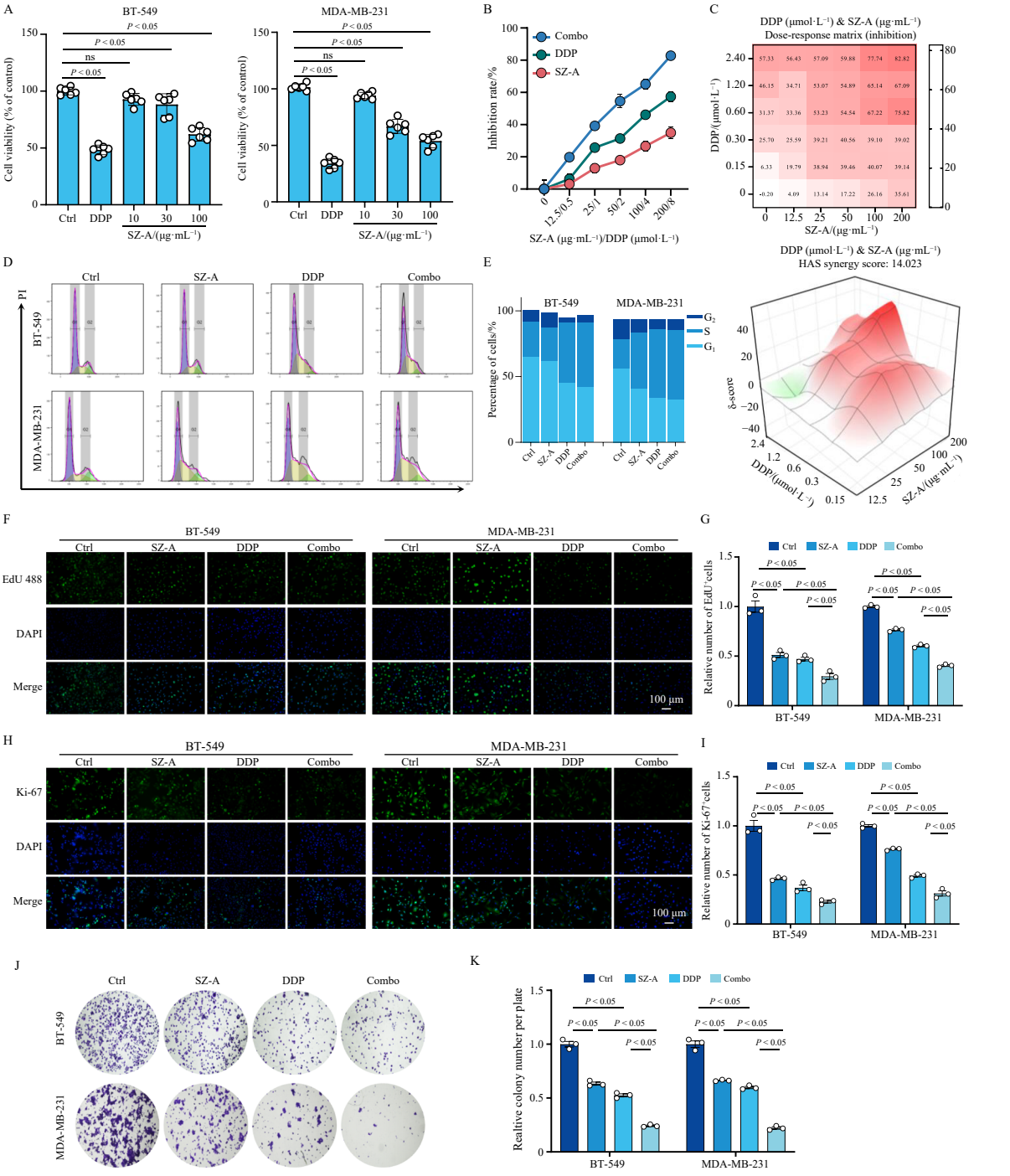


Fig. 1 SZ-A synergistically inhibits TNBC cell proliferation with DDP. (A) Cell viability of BT-549 and MDA-MB-231 lines diminished progressively following exposure to a concentration gradient of SZ-A (10, 30, 100 μg·mL^{-1}, n = 6). (B) After 24 h of treatment, both SZ-A and DDP, alone or in combination, inhibited the growth of MDA-MB-231 cells (n = 6). (C) Synergy analysis performed using SynergyFinder+ revealed a synergistic interaction between SZ-A and DDP, with a HAS synergy score of 14.023. SZ-A was evaluated at 0, 12.5, 25, 50, 100, and 200 μg·mL^{-1}, combined with DDP at 0, 0.15, 0.3, 0.6, 1.2, and 2.4 μmol·L^{-1}. (D and E) Cell cycle distribution of BT-549 and MDA-MB-231 cells after 24 h combination treatment, showing arrest in S phase. (F and G) EdU incorporation assay showing reduced proliferation in BT-549 and MDA-MB-231 cells following 24 h combination treatment. (H and I) After 24 h of treatment with SZ-A and DDP, the Ki-67 positivity rate of BT-549 and MDA-MB-231 cells significantly decreased. (J and K) Colony formation assay demonstrating impaired clonogenic survival of BT-549 and MDA-MB-231 cells after 24 h combination treatment. For all graphs, unless otherwise specified, the data are presented as mean ± SEM of three independent experiments. Statistical analyses were conducted utilizing one-way ANOVA.

from GeneCards, DisGeNET, and OMIM databases. Concurrently, putative targets of the core bioactive constituents of SZ-A (DNJ, FA and DAB) were predicted using SwissTargetPrediction (Fig. 3A). Intersection analysis identified 52 overlapping targets between TNBC and SZ-A, including MAGM, GLA, and PLA2G2A (Fig. 3B). KEGG and GO enrichment analyses revealed significant association of these targets with lipid metabolism, carbohydrate metabolism, and sphingolipid signaling pathways (Figs. 3C and 3D). Notably, PLA2G2A emerged as a high-ranking candidate in the target screening of SZ-A and was found to be implicated in lipid metabolism (Fig. 3E). These findings suggest that SZ-A may modulate lipid homeostasis through PLA2G2A-mediated mechanisms, potentially influencing the progression of TNBC.

3.3. SZ-A stabilizes PLA2G2A by inhibiting autophagic-lysosomal degradation

Analysis of TCGA breast invasive carcinoma data confirmed significant downregulation of PLA2G2A in tumor tissues versus adjacent normal controls (Fig. 4A). Elevated PLA2G2A expres-

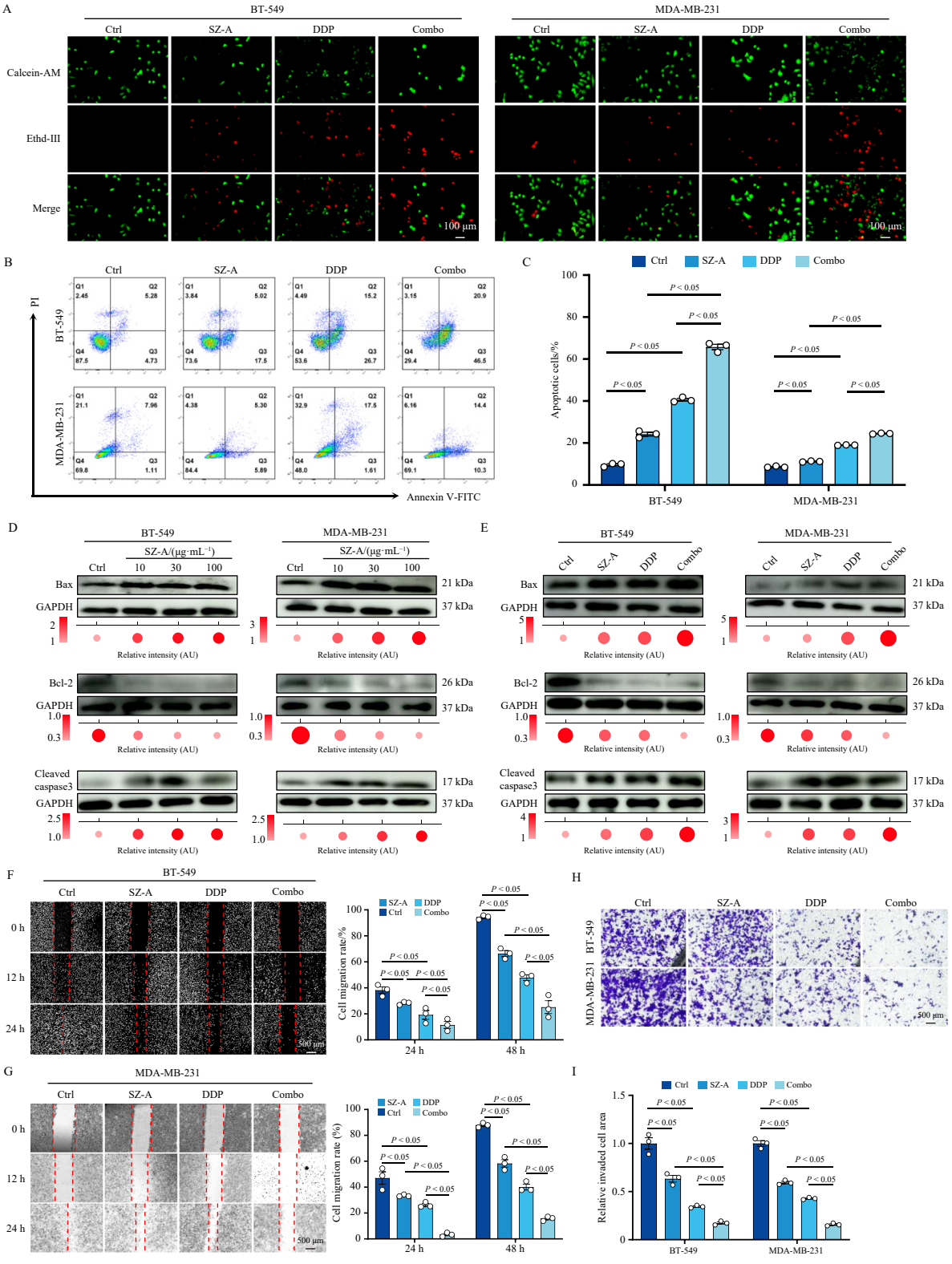


Fig. 2 SZ-A synergistically enhances DDP-induced apoptosis and suppresses malignant phenotypes. (A) Live/dead cell staining (calcein AM, green; EthD-III, red) showing reduced viability of BT-549 and MDA-MB-231 cells following treatment with SZ-A and DDP. (B and C) Annexin V/PI flow cytometry showed elevated apoptosis rates in BT-549 and MDA-MB-231 cells following SZ-A and DDP treatment. (D) Western blot analysis of apoptosis-related proteins in BT-549 and MDA-MB-231 cells treated with SZ-A, showing upregulation of Bax and cleaved caspase-3 and downregulation of Bcl-2. (E) Combination treatment with SZ-A and DDP further modulated the protein levels of Bax, Bcl-2, and cleaved caspase-3 in BT-549 and MDA-MB-231 cells. (F and G) Wound healing assay demonstrating impaired migration of BT-549 (F) and MDA-MB-231 (G) cells after 12 and 24 h treatment with SZ-A and DDP. (H and I) Transwell invasion assay showing suppressed invasion of BT-549 (H) and MDA-MB-231 (I) cells after 24 h treatment with SZ-A and DDP. Data are presented as mean ± SEM of three independent experiments. Statistical analyses were conducted utilizing one-way ANOVA.

sion correlated with improved overall survival in GSE2034 (P = 0.035) and GSE3494 (P = 0.028) cohorts (Figs. 4B and 4C). Pathway enrichment analysis revealed positive association with apoptosis ($\rho_{spearman}$ = 0.38, P = 2.80 × 10^{-38}) and inverse correlation with proliferation signatures ($\rho_{spearman}$ = −0.15, P = 2.87 × 10^{-7}), supporting tumor-suppressive role of PLA2G2A (Figs. 4D and 4E).

SZ-A treatment significantly increased PLA2G2A protein, but not mRNA levels in BT-549 and MDA-MB-231 cells (Figs. 4F and 4G), with cycloheximide chase assays demonstrating extended PLA2G2A half-life (Fig. 4H), confirmed SZ-A-mediated stabiliza-

tion of PLA2G2A. Co-treatment with autophagy-lysosome inhibitor chloroquine (CQ) conferred no additional increase of SZ-A-induced PLA2G2A accumulation, whereas proteasome inhibitor MG132 synergistically enhanced PLA2G2A stabilization (Figs. 4I and 4J), establishing that SZ-A stabilizes PLA2G2A by antagonizing autophagic-lysosomal degradation. Molecular docking confirmed high-affinity binding of SZ-A constituents to PLA2G2A's catalytic pocket, while CETSA or DARTS confirmed enhanced protein stability and protease resistance (Figs. 4K–4N). Critically, SZ-A/DDP combination treatment elevated PLA2G2A protein levels 1.4-fold beyond DDP monotherapy (Fig. 4O), concomitant with enhanced apoptosis. These findings indicate that direct PLA2G2A targeting and stabilization constitutes a key mechanism whereby SZ-A potentiates DDP efficacy in TNBC.

3.4. PLA2G2A is essential for SZ-A-mediated suppression of malignant phenotypes in TNBC

Stable PLA2G2A knockdown *via* shRNA significantly increased MDA-MB-231 cell proliferation, clonogenicity, migration, and invasion (Figs. 5A–5K), confirming its tumor-suppressive function. Critically, PLA2G2A knockdown abolished SZ-A-induced phenotypic suppression, as evidenced by the loss of SZ-A efficacy in knockdown cells relative to shNC + SZ-A: EdU^+ cell reduction decreased 4.82-fold, Ki-67^+ nuclei suppression diminished 2.87-fold, colony formation inhibition dropped 2.57-fold, and invaded/migrated areas decreased by 3.39/1.79-fold (Figs. 5A–5K). Cell cycle analysis revealed that PLA2G2A knockdown prevented SZ-A-induced S-phase arrest (Figs. 5L and 5M), while the percentage of Annexin$^+$ V/PI$^+$ cells was reduced from 22.5% to 12.4% (Figs. 5N and 5O). Concomitantly, SZ-A-mediated upregulation of PLA2G2A, Bax and cleaved caspase-3, with Bcl-2 downregulation, was abolished in PLA2G2A-deficient cells (Figs. 5P–5R). These data establish PLA2G2A as the molecular mediator of SZ-A-induced apoptosis in TNBC cells.

3.5. SZ-A inhibits fatty acid oxidation (FAO) via PLA2G2A to drive lipid accumulation in TNBC

Considering the involvement of PLA2G2A in cellular lipid metabolism, we further explored the effects of SZ-A on lipid metabolism in TNBC cells. BODIPY staining revealed that the combination of SZ-A and DDP significantly elevated lipid content in TNBC cells, a finding corroborated by Oil Red O staining (Figs. 6A–6F). Lipid accumulation in tumor cells is predominantly linked to *de novo* fatty acid synthesis and degradation pathways. DDP has been shown to inhibit FAO and reduce the levels of free fatty acids (FFA) in MDA-MB-231 cells, which aligns with prior evidence demonstrating DDP's suppressive effect on tumor lipid metabolism [18]. However, treatment with SZ-A alone did not significantly alter FFA levels. Furthermore, compared to monotherapy, the combination of DDP and SZ-A only further inhibited FAO (Figs. 6G and 6H). Transcriptomic analysis of TNBC specimens in the TCGA cohort revealed no significant correlation between PLA2G2A expression and fatty acid biosynthesis pathways ($\rho_{spearman}$ = 0.13, P > 0.05, Fig. 6I). This was confirmed by PCR, which indicated that SZ-A selectively downregulated the expression of genes associated with FFA oxidation, while having minimal impact on genes related to fatty acid biosynthesis. The combination of SZ-A and DDP only further downregulated the expression of lipid oxidation-related gene compared to monotherapy (Fig. 6J). Knockdown of PLA2G2A elevated FAO flux in MDA-MB-231 cells and concomitantly up-regulated FAO-related transcripts, whereas overexpression of PLA2G2A repressed FAO flux. Notably, SZ-A failed to suppress FAO activity following PLA2G2A knockdown, indicating that SZ-A requires PLA2G2A to modulate lipid catabolism in TNBC cells (Figs. 6K–6M).

3.6. SZ-A reprograms sphingolipid metabolism to drive ceramide accumulation in TNBC

To elucidate the impact of SZ-A on intracellular lipid compos-

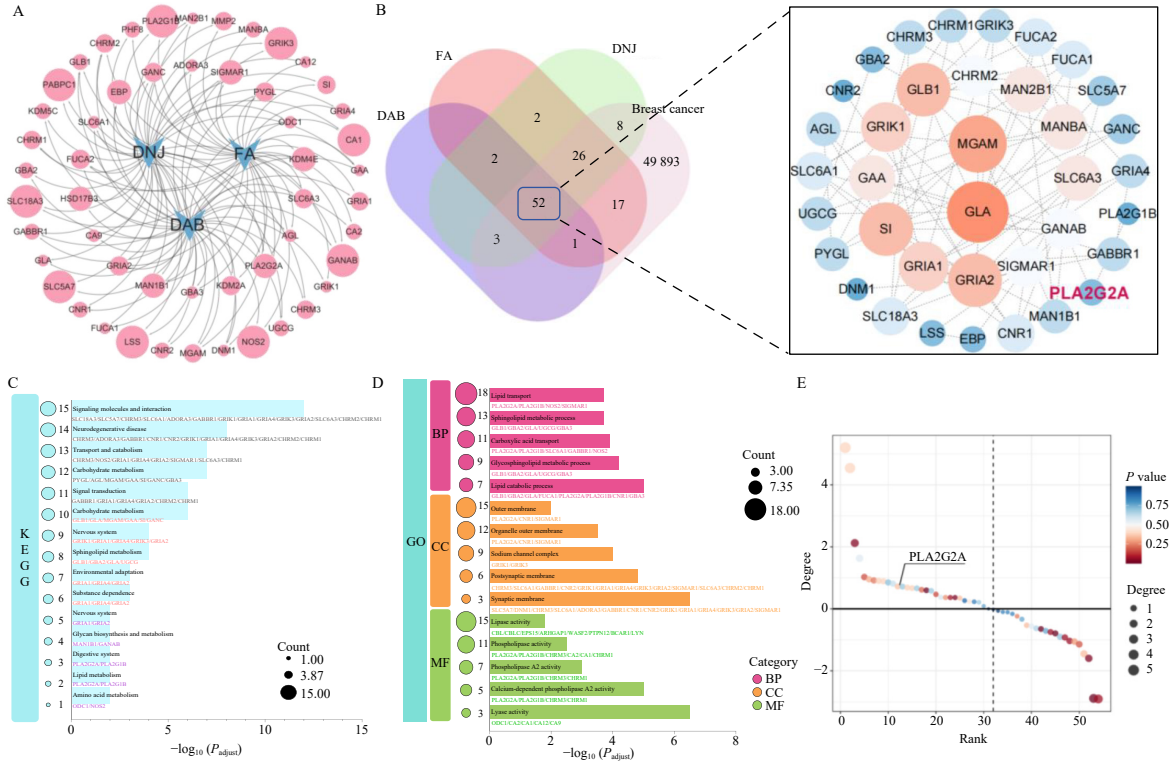


Fig. 3 PLA2G2A is identified as a central mediator of SZ-A-induced apoptosis in TNBC. (A) Dual-layer herb–compound–target–disease interaction network. (B) Venn diagram showing the overlap between major bioactive components of SZ-A and core targets for TNBC treatment, along with the protein–protein interaction network of high-confidence therapeutic targets. (C and D) KEGG (C) and GO (D) pathway enrichment analysis of potential therapeutic targets of SZ-A in TNBC. (E) Ranking of hub targets based on node degree within the interaction network.

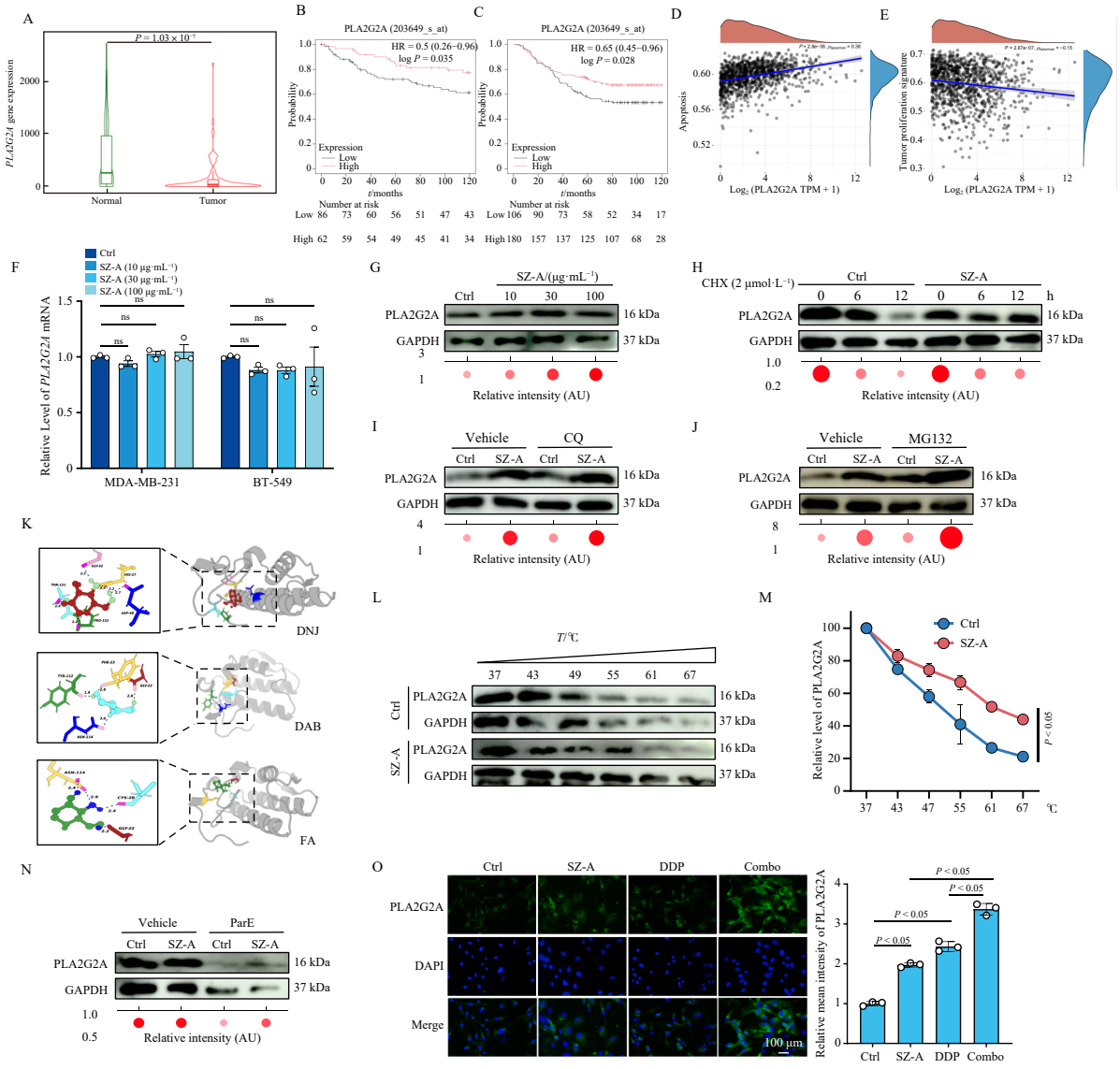


Fig. 4 SZ-A stabilizes PLA2G2A by inhibiting autophagic-lysosomal degradation. (A) Low expression of *PLA2G2A* in breast invasive carcinoma tissues (https://tnmplot.com/analysis/). (B and C) Kaplan-Meier analysis based on GSE3493 (B) and GSE2034 (C) datasets showing that high PLA2G2A expression is associated with improved survival in breast cancer patients (https://kmplot.com/). (D) Positive correlation between PLA2G2A expression and apoptosis-related pathways (www.home-for-researchers.com). (E) Negative correlation between PLA2G2A expression and cell proliferation pathways (www.home-for-researchers.com). (F) *PLA2G2A* mRNA levels in BT-549 and MDA-MB-231 cells are not increased by SZ-A treatment 24 h. (G) Western blot analysis shows a dose-dependent increase in PLA2G2A protein levels in MDA-MB-231 cells treated with SZ-A. (H) Cycloheximide (CHX, 2 μmol·L^{-1}) chase assay in MDA-MB-231 cells shows that SZ-A inhibits PLA2G2A protein degradation. (I) Combined treatment with chloroquine (CQ, 5 μmol·L^{-1}) and SZ-A does not synergistically increase PLA2G2A protein levels. (J) Combined treatment with MG132 (0.3 μmol·L^{-1}) and SZ-A synergistically increases PLA2G2A protein levels in MDA-MB-231 cells. (K) Molecular docking visualization of principal constituents of SZ-A (DNJ, FA, DAB) with the PLA2G2A protein. (L and M) Cellular thermal shift assay (CETSA) showing enhanced thermal stability of PLA2G2A in MDA-MB-231 cells after SZ-A treatment. (N) Drug affinity responsive target stability (DARTS) assay indicating enhanced resistance of PLA2G2A to proteolysis following SZ-A treatment. (O) Immunofluorescence staining reveals maximal upregulation of PLA2G2A in MDA-MB-231 cells after 24 h combined treatment with SZ-A and DDP. Data are presented as mean ± SEM of three independent experiments. Statistical analyses were conducted utilizing one-way ANOVA for F and O, Student's *t*-test for M.

ition and metabolism, we performed untargeted lipidomics analysis. PCA and OPLS-DA demonstrated distinct clustering between the SZ-A and control groups, with significant intergroup separation and robust intragroup clustering, confirming the stability and reliability of the models for subsequent metabolite and pathway analyses (Figs. 7A and 7B). A total of 191 differential lipids were identified in both positive and negative ion modes, comprising 77 upregulated and 114 downregulated lipids (Fig. 7C). KEGG pathway enrichment demonstrated predominant association with sphingolipid metabolism, glycerophospholipid metabolism, and sphingolipid signaling pathways, with divergent directional regulation evidenced by negative enrichment scores for glycerophospholipid metabolism versus positive scores for sphingolipid metabolism (Figs. 7D and 7E). Sphingolipid metabolism was also significantly enriched in our network pharmacology analysis centered on SZ-A, suggesting that SZ-A can modulate sphingolipid metabolism. Given the significant elevation in differential abundance scores for sphingolipid metabolism and sphingolipid signaling pathways, we focused on the effects of SZ-A on sphingolipid metabolism. Ceramides, as representative sphingolipids, are known to promote apoptosis in tumors. Further analysis of differential lipids revealed that SZ-A treatment led to the upregulation of all detected ceramides (Figs. 7F and 7G). ELISA confirmed a significant increase in total ceramide content in TNBC cells treated with SZ-A. Co-treatment with DDP further amplified ceramide levels beyond SZ-A monotherapy, correlating with enhanced apoptotic induction in TNBC cells (Figs. 7H–7K). These results demonstrate that SZ-A can synergize with DDP to promote ceramide contents and induce apoptosis in TNBC cells.

3.7. SZ-A promotes TNBC cell apoptosis via PLA2G2A-dependent modulation of ADIPOR2-mediated ceramide degradation

Next, we investigated the potential role of SZ-A in inducing

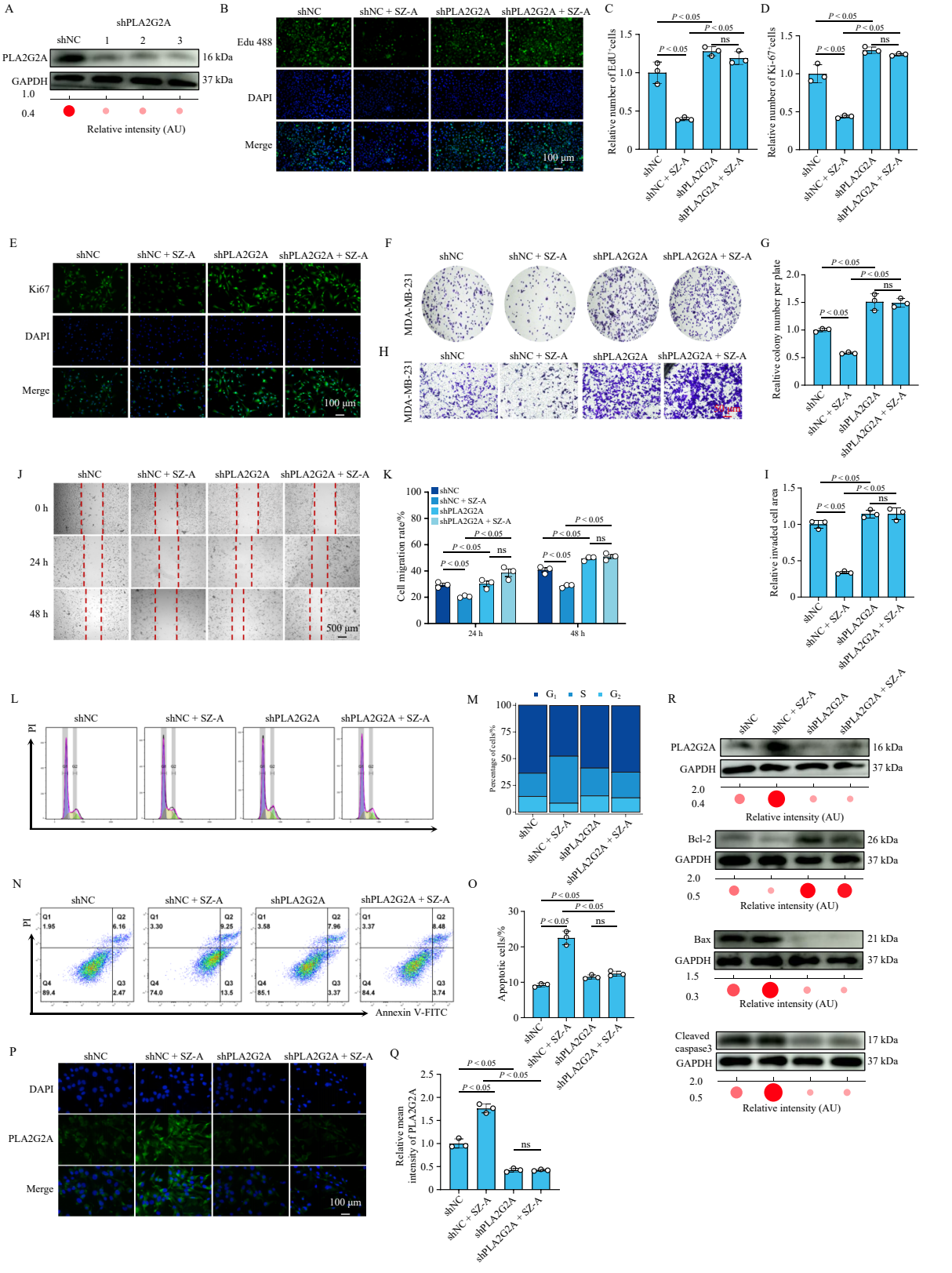


Fig. 5 PLA2G2A is essential for SZ-A-mediated suppression of malignant phenotypes in TNBC. (A) Efficiency validation of knocking down PLA2G2A lentivirus-shRNA. (B–E) PLA2G2A knockdown reverses the inhibitory effect of SZ-A on the proliferation of MDA-MB-231 cells, as measured by EdU (B, C) and Ki-67 (D, E) positivity. (F–I) PLA2G2A knockdown abrogates the SZ-A-mediated suppression of colony formation (F, G) and invasion (H, I) in MDA-MB-231 cells. (J and K) PLA2G2A knockdown abolishes the inhibitory effect of SZ-A on the migration of MDA-MB-231 cells. (L and M) Flow cytometry analysis of cell cycle distribution shows that SZ-A fails to induce S-phase arrest in PLA2G2A-knockdown cells. (N and O) Flow cytometry analysis of apoptosis indicates that PLA2G2A knockdown blocks the pro-apoptotic effect of SZ-A in MDA-MB-231 cells. (P and Q) Immunofluorescence staining of PLA2G2A in control and PLA2G2A-knockdown cells with or without SZ-A treatment. (R) Western blot analysis shows that PLA2G2A knockdown prevents the SZ-A-induced upregulation of PLA2G2A, Bax, and cleaved caspase-3, as well as the downregulation of Bcl-2. Data are presented as mean ± SEM of three independent experiments. Statistical analyses were conducted utilizing one-way ANOVA.

cellular apoptosis *via* the regulation of ceramide mediated by PLA2G2A. PLA2G2A knockdown reduced cellular ceramides, whereas overexpression yielded a marked accumulation (Figs. 8A and 8B), establishing PLA2G2A as a determinant of ceramide

homeostasis. PLA2G2A overexpression also amplified TNF-α-induced ceramide synthesis, indicating regulation of ceramide degradation rather than biosynthesis (Figs. 8C and 8D). Instead, we hypothesize that PLA2G2A may impact ceramide degradation. Ceramides can be hydrolyzed to sphingosine by acid ceramidase (ASAH1) and adiponectin receptors (ADIPOR1/2) [19-22]. Analysis of TCGA breast cancer data revealed no significant correlation between PLA2G2A and ASAH1 expression but exhibited negative correlations with ADIPOR1 and ADIPOR2 (Figs. 8E–8G). PLA2G2A overexpression combined with ASAH1 inhibitor carmofur or ADIPOR1 silencing further increased ceramide levels, whereas ADIPOR2 silencing abolished this enhancement (Figs. 8H–8J). These findings indicate that PLA2G2A-induced ceramide accumulation is ADIPOR2-dependent. SZ-A co-treatment with ADIPOR1 silencing, TNF-α, or carmofur induced cleaved caspase-3 upregulation, but ADIPOR2 silencing prevented additional ceramide accumulation and cleaved caspase-3 elevation beyond SZ-A monotherapy (Figs. 8K–8R). Crucially, these manipulations did not alter PLA2G2A expression (Fig. 8S). These results establish that SZ-A-induced apoptosis concomitant with ADIPOR2-dependent ceramide dynamics.

3.8. SZ-A suppresses TNBC tumor progression through PLA2G2A-dependent ceramide accumulation in vivo

To validate PLA2G2A-dependent ceramide accumulation as the mechanism of SZ-A-induced apoptosis *in vivo*, we established PLA2G2A-knockdown MDA-MB-231 xenografts, and administered SZ-A at a dose of 50 mg·kg^{-1} for a duration of 4 weeks. Knockdown of PLA2G2A significantly accelerated tumor growth and partially mitigated the tumor-suppressive effects of SZ-A, as confirmed by bioluminescent imaging (Figs. 9A–9C). Excised tumors from PLA2G2A-deficient groups exhibited increased volume and weight relative to control cohorts (Figs. 9D–9F). SZ-A-in-

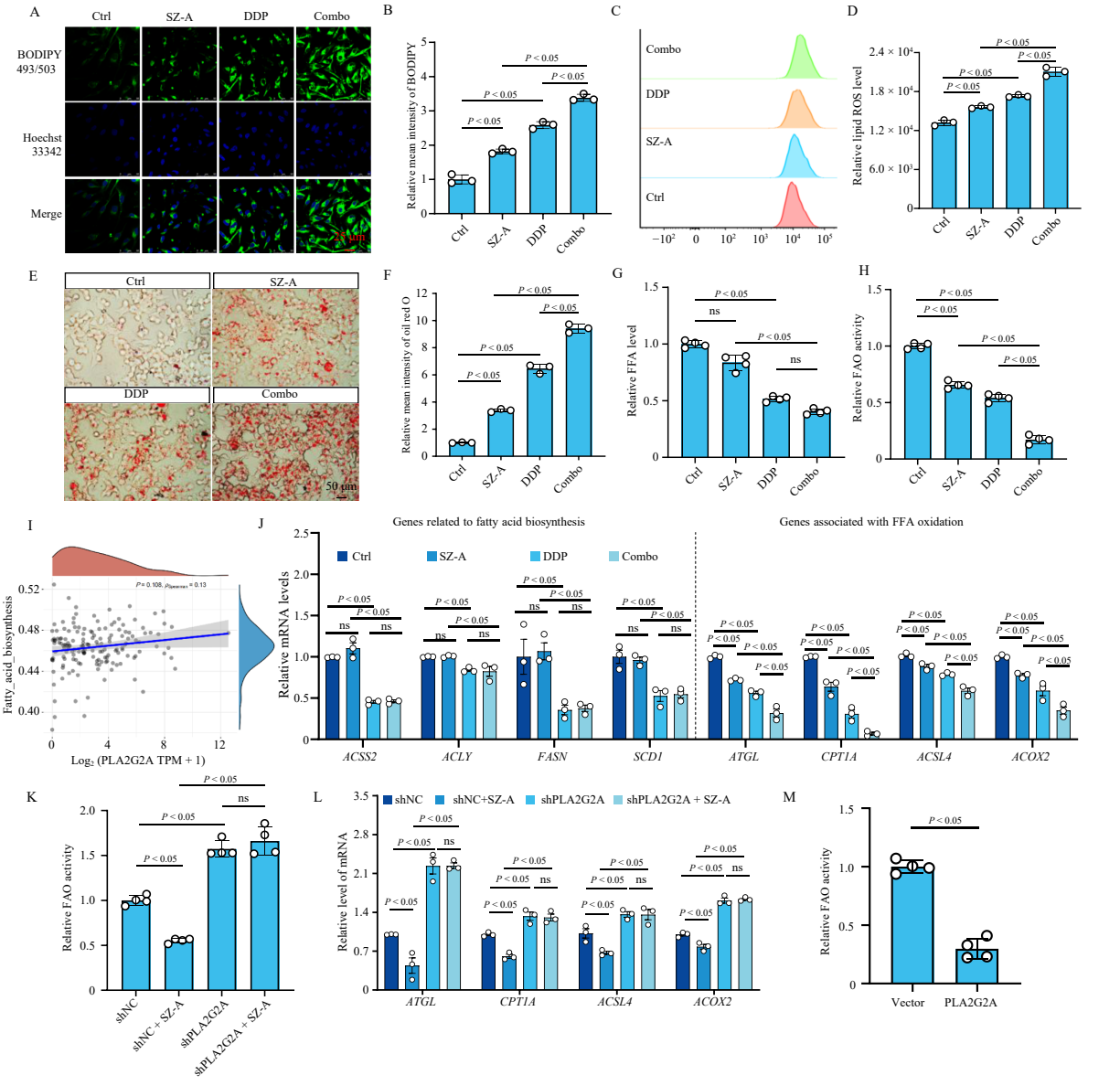


Fig. 6 SZ-A inhibits FAO *via* PLA2G2A to drive lipid accumulation in TNBC. (A and B) BODIPY 493/503 fluorescence staining revealed that the combination of SZ-A and DDP significantly enhances intracellular lipid accumulation in MDA-MB-231 cells. (C and D) Flow cytometry analysis of BODIPY 493/503 fluorescence confirms elevated lipid levels in MDA-MB-231 cells following SZ-A/DDP treatment. (E and F) Oil Red O staining corroborated the significant promotion of intracellular lipid deposition following SZ-A/DDP administration. (G and H) Free fatty acid (FFA, G) and fatty acid oxidation (FAO, H) levels in MDA-MB-231 cells after 24-h treatment with SZ-A, DDP, or SZ-A/DDP. (I) Analysis of the TCGA BRCA cohort reveals no significant correlation between PLA2G2A expression and fatty acid biosynthesis pathway activity (P = 0.108). (J) mRNA levels of key lipid metabolism genes (*ACSS2*, *ACLY*, *FASN*, *SCD1*, *ATGL*, *CPT1A*, *ACSL4*, *ACOX2*) in MDA-MB-231 cells after indicated treatments. (K) PLA2G2A knockdown rescues the SZ-A-mediated suppression of FAO in MDA-MB-231 cells. (L) PLA2G2A knockdown abrogates the downregulation of FAO-related genes (*ATGL*, *CPT1A*, *ACSL4*, *ACOX2*) induced by SZ-A. (M) Overexpression of PLA2G2A suppresses FAO in MDA-MB-231 cells. Data are presented as mean ± SEM of three independent experiments. Statistical analyses were conducted utilizing one-way ANOVA for B, D, F–H, and J–L, Student's *t*-test for M.

duced upregulation of PLA2G2A protein, downregulation of Ki-67-positive cell count and apoptotic activation were abolished in PLA2G2A-knockdown tumors, concomitant with significantly reduced ceramide levels that remained unaltered following SZ-A treatment (Figs. 9G–9K). These observations confirm the essential role of PLA2G2A-mediated ceramide accumulation in SZ-A-driven tumor suppression.

3.9. SZ-A and DDP synergistically inhibit TNBC progression in vivo

Finally, we evaluated the combinatorial efficacy of SZ-A and DDP against TNBC xenografts. Co-treatment significantly sup-

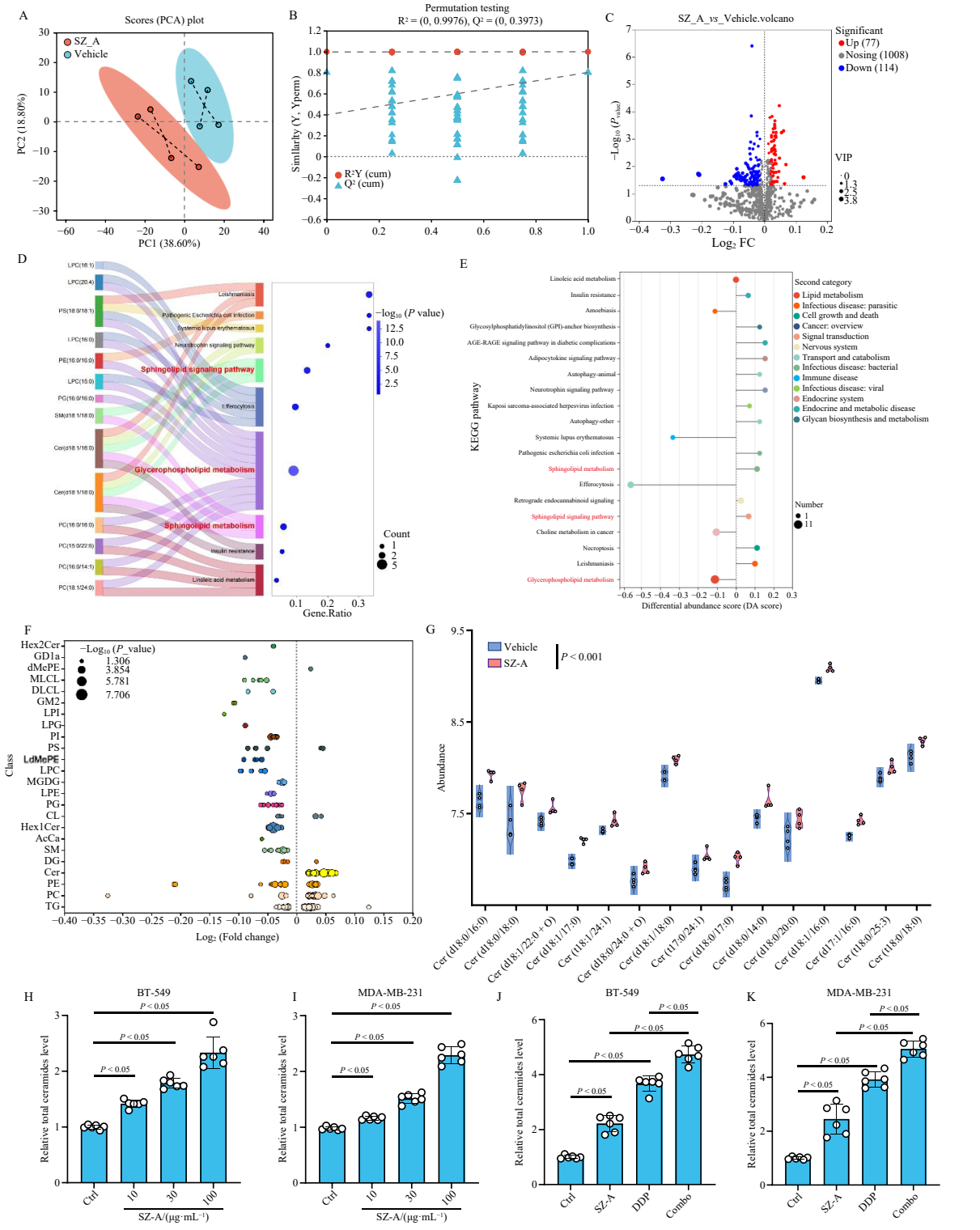


Fig. 7 SZ-A reprograms sphingolipid metabolism to drive ceramide accumulation in TNBC. (A) Principal components analysis (PCA) score plot of metabolomic profiles. (B) Partial least squares discrimination analysis (PLS-DA) score plot. (C) Volcano plot of differential metabolites. The X-axis indicates $\log_2$ (Fold change) and the Y-axis shows the -$\log_{10}$ (*P*-value). (D) KEGG pathway enrichment analysis. Pathways related to lipid metabolism are highlighted in red. (E) Differential abundance (DA) score plot of KEGG metabolic pathways. The X-axis represents the DA score, and the Y-axis shows pathway names. (F) Classification and distribution of significantly altered lipids. (G) Abundance distribution of differential ceramides between Vehicle/SZ-A groups. (H and I) Total ceramide content increases in a dose-dependent manner in BT-549 (H) and MDA-MB-231 (I) cells treated with SZ-A. (J and K) DDP and SZ-A combination synergistically increases total ceramide content in BT-549 (J) and MDA-MB-231 (K) cells. Data are presented as mean ± SEM; $n = 4$ independent experiments for (A–G), $n = 6$ for (H–K). Statistical analyses were conducted utilizing one-way Student's *t*-test for G, ANOVA for H–K.

pressed tumor growth compared to monotherapy regimens, evidenced by marked reductions in flux of bioluminescence, tumor volume and weight (Figs. 10A–10G). This treatment cohort exhibited elevated apoptotic activity concomitant with increased ceramide levels, PLA2G2A expression, and pro-apoptotic markers including Bax and cleaved caspase-3, alongside reduced Bcl-2 expression and Ki-67 proliferation indices (Figs. 10H–10L). Notably, co-treated mice maintained stable body weights comparable to untreated controls and SZ-A monotherapy groups, with no significant weight loss observed during the treatment period

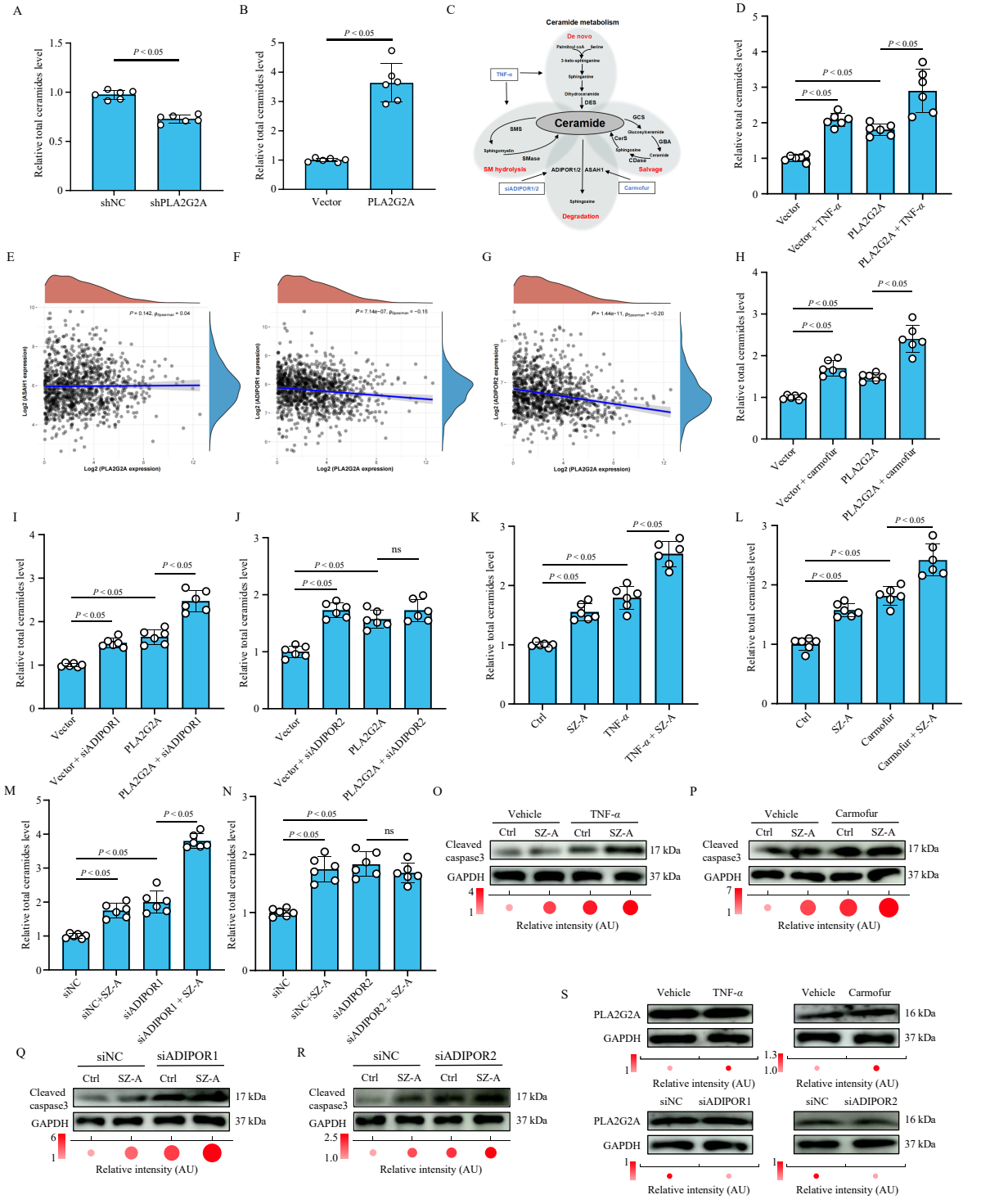


Fig. 8 SZ-A promotes TNBC cell apoptosis *via* PLA2G2A-dependent modulation of ADIPOR2-mediated ceramide degradation. (A and B) Ceramide levels following modulation of PLA2G2A expression. Knockdown of PLA2G2A reduces ceramide levels (A), whereas its overexpression elevates them (B). (C) Schematic diagram of ceramide metabolism and related enzyme modulators. (D) TNF-α treatment leads to a further increase in ceramide content in MDA-MB-231 cells overexpressing PLA2G2A. (E–G) Correlation analysis of PLA2G2A with ASAH1 (E), ADIPOR1 (F), and ADIPOR2 (G) in the TCGA breast cancer cohort. PLA2G2A expression shows no significant correlation with ASAH1 (P = 0.142) but is negatively correlated with both ADIPOR1 and ADIPOR2. (H) Carmofur treatment leads to a further increase in ceramide content in MDA-MB-231 cells overexpressing PLA2G2A. (I and J) Ceramide levels in PLA2G2A-overexpressing MDA-MB-231 cells after individual knockdown of ADIPOR1 or ADIPOR2. siADIPOR1 enhances ceramide accumulation, while siADIPOR2 shows no effect. (K and L) Co-treatment with SZ-A and TNF-α (K) or carmofur (L) significantly elevates ceramide levels in MDA-MB-231 cells. (M and N) Effect of SZ-A on ceramide levels in ADIPOR1/2-knockout MDA-MB-231 cells. SZ-A synergizes with ADIPOR1 knockdown to further increase ceramide content (M), whereas its effect in ADIPOR2-knockout cells is merely additive (N). (O–R) Cleaved caspase-3 expression after treatment with SZ-A combined with TNF-α, carmofur, or siADIPOR1/2. (S) PLA2G2A protein levels remain unaltered by treatment with TNF-α, carmofur, or ADIPOR1/2 knockdown. Data are presented as mean ± SEM; n = 6 independent experiments for (A, B, D and H–N), n = 4 for (O–S). Statistical analyses were conducted utilizing Student's t-test for A and B, one-way ANOVA for D and H–N.

(Fig. 10M). These results demonstrate that SZ-A synergizes with DDP to activate the PLA2G2A-ceramide axis, inducing apoptosis while reducing chemotherapy toxicity, ultimately suppressing TNBC progression.

4. Discussion

Despite the approval of poly ADP ribose polymerase inhibitors, immune checkpoint inhibitors, and antibody-drug conjugates for the treatment of TNBC, chemotherapy agents such as anthracyclines, taxanes, and platinum compounds continue to be the cornerstone of TNBC therapy [23, 24]. This reliance is primarily due to the paucity of therapeutic targets and the emergence of drug resistance. Nonetheless, these conventional treatments are frequently associated with considerable toxic side effects and a high propensity for resistance, underscoring the critical need for novel therapeutic strategies [25]. Here we show that the potential of an extract from the traditional Chinese medicine, SZ-A, to act synergistically with DDP in inhibiting the progression of TNBC.

SZ-A, an approved *α*-glucosidase inhibitor for T2DM mechanistically analogous to acarbose, exhibits reported anti-tumor properties including glucose deprivation-dependent cytotoxicity and gut microbiota-mediated enhancement of immunotherapy efficacy *via* tryptophan metabolism modulation [26]. Given the well-

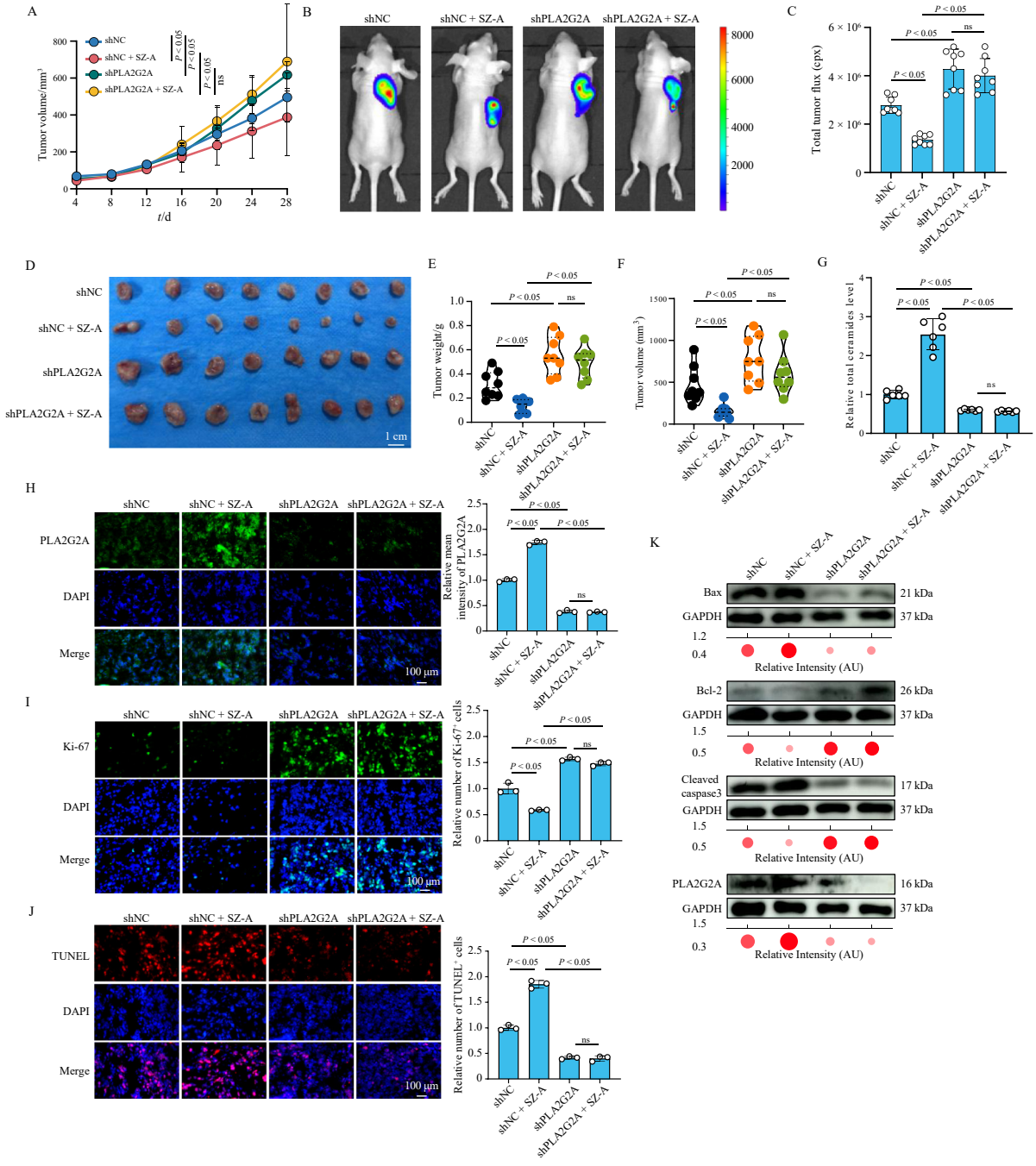


Fig. 9 SZ-A suppresses TNBC tumor progression through PLA2G2A-dependent ceramide accumulation *in vivo*. (A) Xenograft tumors derived from PLA2G2A-knockdown MDA-MB-231 cells show no response to SZ-A treatment (50 mg·kg^{-1}, 4 weeks). (B and C) *In vivo* imaging showing that PLA2G2A knockdown promoted tumor growth and attenuated the antitumor effect of SZ-A. (D) Representative tumor images from each group. (E and F) Tumor weight (E) and volume (F) in mice with PLA2G2A knockdown and SZ-A treatment. (G) PLA2G2A knockdown abrogates the SZ-A-induced increase in tumor ceramide content. (H) Immunofluorescence staining of PLA2G2A in tumor tissues. (I) PLA2G2A knockdown reverses the SZ-A-mediated reduction of Ki-67 positive cells in tumors. (J) PLA2G2A knockdown reverses the SZ-A-mediated increased of TUNEL positive cells in tumors. (K) SZ-A elevates pro-apoptotic Bax, PLA2G2A and cleaved caspase-3, while concomitantly repressing Bcl-2 in shNC tumors; knockdown of PLA2G2A inverts this profile. Data are presented as mean ± SEM; n = 8 independent experiments for (A–G), n = 4 for (H–K). Statistical analyses were conducted utilizing one-way ANOVA.

established interconnections between carbohydrate and lipid metabolic pathways in oncogenesis, and the known lipid regulatory capacity of acarbose [27-29], we sought to investigate whether SZ-A possesses similar anti-tumor activity. Our findings demonstrate SZ-A induces apoptosis in TNBC cells, although monotherapy yields insufficient efficacy at clinically relevant doses. Nonetheless, SZ-A synergizes with DDP, enabling potent tumor suppression at reduced chemotherapeutic exposure. Network pharmacology analysis implicates PLA2G2A as a putative SZ-A target, influencing lipid and sphingolipid metabolism in breast cancer. However, our study did not explore whether SZ-A could affect the progression of TNBC through the regulation of carbohydrate metabolism. This area warrants further investigation to fully elucidate the multifaceted mechanisms by which SZ-A exerts its anti-tumor effects.

PLA2G2A exhibits low expression levels in breast cancer. Elevated PLA2G2A correlates with improved overall survival in breast cancer, yet it is highly expressed in gastric cancer and promotes *de novo* lipogenesis and energy metabolism to drive proliferation in K-Ras-mutant pancreatic ductal adenocarcinoma, where it is therapeutically targeted by inhibitors like tanshinone I [30]. In this study, we uncover a novel mechanism by which PLA2G2A is regulated in TNBC: SZ-A directly binds PLA2G2A, inhibiting its lysosomal degradation and inducing post-translational stabilization. This results in suppressed lipid oxidation and consequent intracellular lipid accumulation, independent of effects on *de novo* fatty acid synthesis. In contrast, DDP concurrently inhibits both *de novo* lipogenesis and fatty acid oxidation.

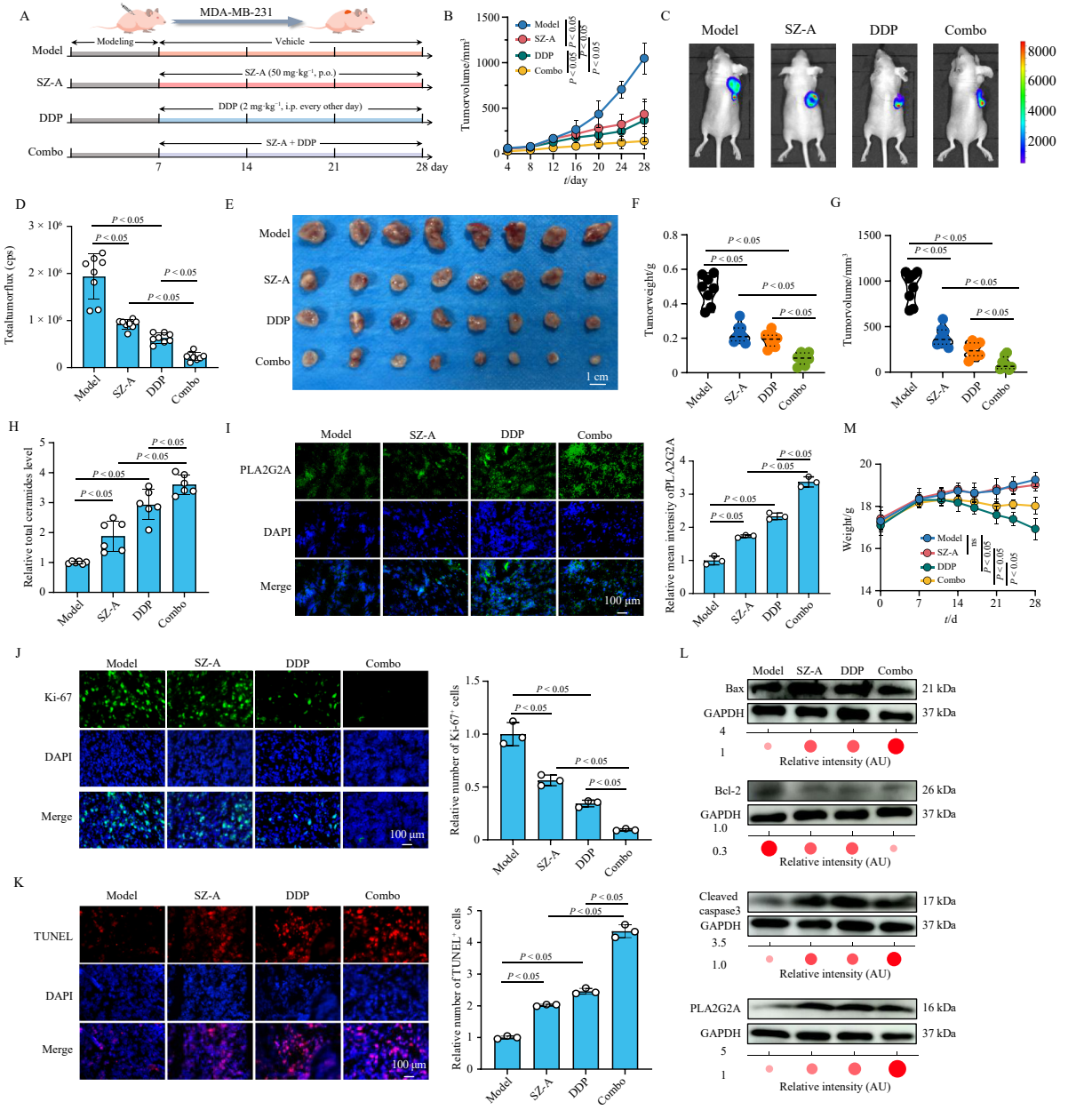


Fig. 10 SZ-A and DDP synergistically inhibit TNBC progression *in vivo*. (A) Experimental timeline for tumor induction and treatment in mice. (B) Tumor growth curves in mice treated as indicated [vehicle, SZ-A (50 mg·kg^{-1}), DDP (2 mg·kg^{-1}), or combination]. The SZ-A/DDP combination exhibits potent anti-tumor activity. (C and D) *In vivo* imaging showing suppression of tumor growth following combination treatment with SZ-A and DDP. (E) Representative images of excised tumor tissues. (F and G) Compared to single-agent treatments, the SZ-A/DDP combination shows significantly greater efficacy in reducing tumor weight (F) and volume (G). (H) Combination treatment with SZ-A and DDP elevates tumor ceramide levels beyond those achieved with monotherapy. (I) Immunofluorescence staining of PLA2G2A in tumor tissues. (J) Ki-67-positive tumor cells are synergistically decreased by the SZ-A/DDP combination relative to single-agent treatment. (K) The combination treatment yields a greater increase in TUNEL-positive cells than either SZ-A or DDP alone. (L) Western blot analysis of Bax, Bcl-2, PLA2G2A, and cleaved caspase-3 expression in tumor tissues. (M) Body weight changes in mice during modeling and treatment. Data are presented as mean ± SEM; n = 8 independent experiments for (B–H and M), n = 4 for (I–L). Statistical analyses were conducted utilizing one-way ANOVA.

The complementary metabolic blockade, SZ-A impairing lipid catabolism and DDP disrupting anabolic/catabolic pathways, provides a mechanistic basis for their synergistic suppression of TNBC progression.

Inhibition of FAO drives intracellular lipid accumulation [31]. Lipidomic profiling revealed that SZ-A treatment significantly reduces glycerophospholipid species. This depletion attenuates fatty acid flux into phospholipid biosynthesis, resulting in cytosolic retention of fatty acids that would otherwise be incorporated into membrane lipids [32]. While FAO represents the primary catabolic pathway for surplus fatty acids, this route is paradoxically suppressed by SZ-A. Critically, we observe concomitant elevation of ceramides, indicating a metabolic rerouting wherein accumulated fatty acids are preferentially channelled into *de novo* sphingolipid biosynthesis [33]. Thus, SZ-A-mediated blockade of fatty acid oxidation drives fatty acid diversion into the ceramide metabolic pathway, culminating in minimal net change in free fatty acid pools but pathological ceramide accumulation.

Ceramides function as signaling molecules, orchestrating critical physiological processes such as energy homeostasis and cell death through pleiotropic mechanisms [34, 35]. Stress-induced ceramide accumulation drives cancer cell demise *via* apoptosis, necroptosis, autophagy, and oxidative stress [36]. A prevailing mechanistic paradigm posits that ceramides self-assemble into barrel-stave pores within the mitochondrial outer membrane, thereby increasing permeabilization and releasing cytochrome C, SMAC/DIABLO, and other pro-apoptogenic factors to initiate the caspase-mediated apoptotic cascade [37, 38]. Increased generation of C14∶0, C16∶0, and C18∶0 ceramides *via* ceramide synthase 6 (CERS6) overexpression antagonizes mTOR signaling and curtails proliferation in MCF-7 breast cancer cells [39]. Microbial riboflavin produced by the gut microbiota also inhibits CERS3-dependent synthesis of very-long-chain ceramides (d18∶1/26∶0) and EGFR signaling, and restrains colorectal cancer progression [40]. This aligns with our observations linking ceramide accumulation to apoptosis induction and proliferation arrest.

Ceramide accumulation arises from imbalances in biosynthesis versus degradation. Mammalian ceramide, a major plasma membrane sphingolipid, is *de novo* synthesized at the ER cytosolic leaflet *via* sequential catalysis by serine palmitoyltransferase (SPT), CerS, and dihydroceramide desaturase, utilizing palmitoyl-CoA and L-serine [41]. Degradation of ceramide, on the other hand, is regulated by enzymes such as ASAH1 and ADIPOR1/2, which hydrolyze ceramide into sphingosine and FFAs. Sphingosine can be further metabolized to sphingosine-1-phosphate (S1P) by sphingosine kinase, thereby influencing cellular signaling pathways [20-22]. Inflammatory stimuli, including TLR4 agonists, TNF-α, and interleukins, elevate ceramide by inducing *de novo* biosynthetic enzymes and activating sphingomyelinases, while ASAH1 inhibitors like camofur promote apoptosis by blocking degradation. Critically, we demonstrate that TNF-α, camofur, and ADIPOR1 knockdown functionally synergize with SZ-A to amplify ceramide synthesis in TNBC. However, ADIPOR2 knockdown uniquely abrogated SZ-A-driven ceramide accumulation, establishing ADIPOR2 signaling as the essential conduit for SZ-A's ceramide-elevating effect downstream of PLA2G2A. While the salvage pathway represents an additional ceramide source, the impact of SZ-A/PLA2G2A on salvage enzymes and key *de novo* factors, like SPT or CerS, remains undefined. In addition, the molecular mechanism by which PLA2G2A regulates ADIPOR2, such as affecting its activity or expression, also requires further investigation.

5. Conclusion

In summary, our study demonstrates that SZ-A directly targets PLA2G2A, enhancing its protein stability and modulating FAO. This interaction inhibits ceramide degradation, leading to intracellular ceramide accumulation, induction of apoptosis, and subsequent suppression of TNBC progression. Our findings define a novel chemosensitization strategy through pharmacological activation of the PLA2G2A-ceramide axis, thereby significantly enhancing DDP efficacy in refractory TNBC and highlighting its potential to improve outcomes for patients with limited options.

Funding

This work was supported by the National Natural Science Foundation of China (Nos. 82270879 and 82504844), the Foundation of Excellent Youth Scholars of Education Committee of Anhui Province of China (No. 2022AH030124), the Key Project of Natural Science Foundation of the Department of Education of Anhui Province (No. 2025AHGXZK31285).

Declaration of interest statement

These authors have no conflict of interest to declare.

References

1 Jie H, Ma W, Huang C. Diagnosis, prognosis, and treatment of triple-negative breast cancer: a review. *Breast Cancer (Dove Med Press)*. 2025;17:265-274. https://doi.org/10.2147/bctt.S516542.
2 Zhu Y, Hu Y, Tang C, et al. Platinum-based systematic therapy in triple-negative breast cancer. *Biochim Biophys Acta Rev Cancer*. 2022;1877(1): 188678. https://doi.org/10.1016/j.bbcan.2022.188678.
3 Chen T, Xiao Z, Liu X, et al. Natural products for combating multidrug resistance in cancer. *Pharmacol Res*. 2024;202:107099. https://doi.org/10.1016/j.phrs.2024.107099.
4 Chen Y, Jiang X, Xie H, et al. Structural characterization and antitumor activity of a polysaccharide from Ramulus Mori. *Carbohydr Polym*. 2018;190: 232-239. https://doi.org/10.1016/j.carbpol.2018.02.036.
5 An X, Yang X, Ding X, et al. Ramulus Mori (Sangzhi) alkaloids tablets for diabetes mellitus: a regulatory perspective. *Fitoterapia*. 2023;166:105444. https://doi.org/10.1016/j.fitote.2023.105444.
6 Liu W, Xu S, Zhang B, et al. Ramulus Mori (Sangzhi) alkaloids alleviate diabetic nephropathy through improving gut microbiota disorder. *Nutrients*. 2024;16(14):2346. https://doi.org/10.3390/nu16142346.
7 Shang X, Fu Y, Wang Y, et al. Ramulus Mori (Sangzhi) alkaloids ameliorate high-fat diet induced obesity in rats by modulating gut microbiota and bile acid metabolism. *Front Endocrinol (Lausanne)*. 2024;15:1506430. https://doi.org/10.3389/fendo.2024.1506430.
8 Liu D, Ye J, Yan Y, et al. Ramulus Mori (Sangzhi) alkaloids regulates gut microbiota disorder and its metabolism profiles in obese mice induced by a high-fat diet. *Front Pharmacol*. 2023;14:1166635. https://doi.org/10.3389/fphar.2023.1166635.
9 Xiao Q, Xia M, Tang W, et al. The lipid metabolism remodeling: a hurdle in breast cancer therapy. *Cancer Lett*. 2024;582:216512. https://doi.org/10.1016/j.canlet.2023.216512.
10 Sevastou I, Kaffe E, Mouratis MA, et al. Lysoglycerophospholipids in chronic inflammatory disorders: the PLA(2)/LPC and ATX/LPA axes. *Biochim Biophys Acta*. 2013;1831(1):42-60. https://doi.org/10.1016/j.bbalip.2012.07.019.
11 Ge W, Yue M, Lin R, et al. PLA2G2A$^{(+)}$ cancer-associated fibroblasts mediate pancreatic cancer immune escape *via* impeding antitumor immune response of CD8$^{(+)}$ cytotoxic T cells. *Cancer Lett*. 2023;558:216095. https://doi.org/10.1016/j.canlet.2023.216095.
12 Wang M, Hao FY, Wang JG, et al. Group IIa secretory phospholipase A2 (sPLA2IIa) and progression in patients with lung cancer. *Eur Rev Med Pharmacol Sci*. 2014;18(18):2648-2654.
13 Bedir I, Ozturk K, Telci D. Impact of PLA2G2A rs11573156 C > G variant on phospholipase expression and metastatic behavior in prostate cancer. *Gene*. 2025;964:149641. https://doi.org/10.1016/j.gene.2025.149641.
14 Ozturk K, Onal MS, Efiloglu O, et al. Association of 5'UTR polymorphism of secretory phospholipase A2 group IIA (PLA2G2A) gene with prostate cancer metastasis. *Gene*. 2020;742:144589. https://doi.org/10.1016/j.gene.2020.144589.
15 Hatori S, Sakamaki K, Yokohori T, et al. Clinical significance of PLA2G2A expression in gastric cancer patients who receive gastrectomy and adjuvant S-1. *Anticancer Res*. 2021;41(7):3583-3588. https://doi.org/10.21873/anticanres.15146.
16 Shariati M, Aghaei M, Movahedian A, et al. The effect of ω-fatty acids on the expression of phospholipase A(2) group 2A in human gastric cancer patients. *J Res Med Sci*. 2016;21:10. https://doi.org/10.4103/1735-1995.177358.
17 Zhai Z, Mu T, Zhao L, et al. Stachydrine represses the proliferation and enhances cell cycle arrest and apoptosis of breast cancer cells *via* PLA2G2A/DCN axis. *Chem Biol Drug Des*. 2024;103(1):e14429. https://doi.org/10.1111/cbdd.14429.
18 Tan Y, Li J, Zhao G, et al. Metabolic reprogramming from glycolysis to fatty acid uptake and beta-oxidation in platinum-resistant cancer cells. *Nat*

Commun. 2022;13(1):4554. https://doi.org/10.1038/s41467-022-32101-w.
19 Dementiev A, Joachimiak A, Nguyen H, et al. Molecular mechanism of inhibition of acid ceramidase by carmofur. *J Med Chem*. 2019;62(2):987-992. https://doi.org/10.1021/acs.jmedchem.8b01723.
20 Vasiliauskaité-Brooks I, Sounier R, Rochaix P, et al. Structural insights into adiponectin receptors suggest ceramidase activity. *Nature*. 2017;544(7648): 120-123. https://doi.org/10.1038/nature21714.
21 Blachnio ZAU, Koutsari C, Tchkonia T, et al. Sphingolipid content of human adipose tissue: relationship to adiponectin and insulin resistance. *Obesity (Silver Spring)*. 2012;20(12):2341-2347. https://doi.org/10.1038/oby.2012.126.
22 Vijayan Y, Lankadasari MB, Harikumar KB. Acid ceramidase: a novel therapeutic target in cancer. *Curr Top Med Chem*. 2019;19(17):1512-1520. https://doi.org/10.2174/1568026619666190227222930.
23 Wagle NS, Nogueira L, Devasia TP, et al. Cancer treatment and survivorship statistics, 2025. *CA Cancer J Clin*. 2025;75(4):308-340. https://doi.org/10.3322/caac.70011.
24 Zhu S, Wu Y, Song B, et al. Recent advances in targeted strategies for triple-negative breast cancer. *J Hematol Oncol*. 2023;16(1):100. https://doi.org/10.1186/s13045-023-01497-3.
25 Wu GY, Xiao MZ, Hao WC, et al. Drug resistance in breast cancer: mechanisms and strategies for management. *Drug Resist Updat*. 2025;83: 101288. https://doi.org/10.1016/j.drup.2025.101288.
26 Zhang SL, Wang X, Cai QQ, et al. Acarbose enhances the efficacy of immunotherapy against solid tumours by modulating the gut microbiota. *Nat Metab*. 2024;6(10):1991-2009. https://doi.org/10.1038/s42255-024-01137-1.
27 Xing Y, Ren X, Li X, et al. Baicalein enhances the effect of acarbose on the improvement of nonalcoholic fatty liver disease associated with prediabetes *via* the inhibition of *de novo* lipogenesis. *J Agric Food Chem*. 2021;69(34): 9822-9836. https://doi.org/10.1021/acs.jafc.1c04194.
28 Göke B. Improved glycemic control and lipid profile in a randomized study of pioglitazone compared with acarbose in patients with type 2 diabetes mellitus. *Treat Endocrinol*. 2002;1(5):329-336. https://doi.org/10.2165/00024677-200201050-00005.
29 Wan M, Pan S, Shan B, et al. Lipid metabolic reprograming: the unsung hero in breast cancer progression and tumor microenvironment. *Mol Cancer*. 2025;24(1):61. https://doi.org/10.1186/s12943-025-02258-1.
30 Zhang M, Xiang R, Glorieux C, et al. PLA2G2A phospholipase promotes fatty acid synthesis and energy metabolism in pancreatic cancer cells with K-ras mutation. *Int J Mol Sci*. 2022;23(19):11721. https://doi.org/10.3390/ijms231911721.
31 Ma J, Wang S, Zhang P, et al. Emerging roles for fatty acid oxidation in cancer. *Genes Dis*. 2025;12(4):101491. https://doi.org/10.1016/j.gendis.2024.101491.
32 Valentine WJ, Hashidate YT, Yamamoto S, et al. Biosynthetic enzymes of membrane glycerophospholipid diversity as therapeutic targets for drug development. *Adv Exp Med Biol*. 2020;1274:5-27. https://doi.org/10.1007/978-3-030-50621-6_2.
33 Sakuragi T, Nagata S. Regulation of phospholipid distribution in the lipid bilayer by flippases and scramblases. *Nat Rev Mol Cell Biol*. 2023;24(8):576-596. https://doi.org/10.1038/s41580-023-00604-z.
34 ummers SA, Chaurasia B, Holland WL. Metabolic messengers: ceramides. *Nature Metab*. 2019;1(11):1051-1058. https://doi.org/10.1038/s42255-019-0134-8.
35 Thakkar H, Vincent V, Chaurasia B. Ceramide signaling in immunity: a molecular perspective. *Lipids Health Dis*. 2025;24(1):225. https://doi.org/10.1186/s12944-025-02642-2.
36 Alizadeh J, da Silva RSC, Weng X, et al. Ceramides and ceramide synthases in cancer: focus on apoptosis and autophagy. *Eur J Cell Biol*. 2023;102(3): 151337. https://doi.org/10.1016/j.ejcb.2023.151337.
37 Dadsena S, Zollo C, García-Sáez AJ. Mechanisms of mitochondrial cell death. *Biochem Soc Trans*. 2021;49(2):663-674. https://doi.org/10.1042/bst20200522.
38 Ogretmen B. Sphingolipid metabolism in cancer signalling and therapy. *Nat Rev Cancer*. 2018;18(1):33-50. https://doi.org/10.1038/nrc.2017.96.
39 Kim MH, Park JW, Lee EJ, et al. C16-ceramide and sphingosine 1-phosphate/S1PR2 have opposite effects on cell growth through mTOR signaling pathway regulation. *Oncol Rep*. 2018;40(5):2977-2987. https://doi.org/10.3892/or.2018.6689.
40 Qu R, Zhang Y, Kim B, et al. Microbial riboflavin inhibits ceramide synthase 3 to lower ceramide (d18∶1/26∶0) and delay colorectal cancer progression. *Cell Metab*. 2025;37(9):1852-1869.e8 https://doi.org/10.1016/j.cmet.2025.06.002.
41 Choi RH, Tatum SM, Symons JD, et al. Ceramides and other sphingolipids as drivers of cardiovascular disease. *Nat Rev Cardiol*. 2021;18(10):701-711. https://doi.org/10.1038/s41569-021-00536-1.